ACS OMEGA

Open Access

http://pubs.acs.org/journal/acsodf

Article

Copper-Based Nanoparticles as Precision Nanoantibiotics against Bacterial Blight in *Anthurium andraeanum* Lind.: Synthesis, Characterization, and Antibacterial Efficacy under *In Vitro* and *In Vivo* Conditions

Sanka Wanaguru, Sehan Jayasinghe, Kasun Seneviratne, Nilwala Kottegoda, Sriyani E. Peiris, and Colin N. Peiris*

Cite This: *ACS Omega* 2026, 11, 25657−25665

Read Online

ACCESS | Metrics & More | Article Recommendations | Supporting Information

ABSTRACT: The bacterial blight disease caused by *Xanthomonas* spp., a dilemma for farmers worldwide. The existing conventional methods have failed to effectively combat the disease. Therefore, it is crucial to focus on developing and implementing more affordable techniques to effectively manage bacterial blight effectively. Herein, we investigated the efficacy of copper-based nanoparticles (Cu NPs) synthesized via three different methods toward controlling bacterial blight disease in *Anthurium andraeanum* plants. For that, Cu NPs were engineered via chemical, semichemical, and green synthesis approaches. Cu NPs were characterized through scanning electron microscope (SEM), transmission electron microscope (TEM), Fourier-transform infrared (FTIR), and powder X-ray diffraction (PXRD) analysis. Quantitative antibacterial assays revealed that the chemical and green-synthesized Cu NPs exhibited the highest potency, with a minimum inhibitory concentration (MIC) of 31.25 μg/mL and a minimum bactericidal concentration (MBC) of 62.50 μg/mL, whereas the semichemical formulation showed lower activity (MIC = 62.50 μg/mL; MBC = 125 μg/mL). *In vitro* well-diffusion assays further supported this trend: at 30 ppm, the inhibition zones measured 25 ± 0.81, 15 ± 0.81, and 20.6 ± 0.94 mm for the chemical, semichemical, and green synthesis methods, respectively, compared to 26.3 ± 0.47 mm for the positive control-antibiotic sulfamethoxazole. At *in vivo*, optimized concentration of 200 ppm, Cu NPs produced via all three methods controlled bacterial blight disease in 90% of treated anthurium plants within 4, 7, and 5 weeks, respectively, without causing phytotoxicity. Disease progression was monitored over 12 weeks by measuring lesion areas, and statistical significance of treatments was determined using two-way analysis of variance (ANOVA).

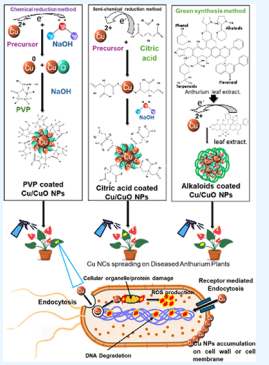

1. INTRODUCTION

The bacterial blight disease caused by *Xanthomonas* spp. poses a significant challenge for most crop varieties worldwide including rice,[1] pomegranate[2,3] and olive.[4] Conventional methods such as field sanitation, antibiotics, chemical treatments,[5] crop rotation, soil solarization, and the use of resistant varieties[6] have shown limited effectiveness in combating the disease.[7] Bacterial blight not only threatens staple crops but also poses a major economic risk to the global horticulture and floriculture industry. The global floriculture market, valued at over 55 billion US Dollars in 2023 and projected to exceed 85 billion US Dollars by 2032, faces significant challenges from such diseases, which can cause severe yield losses, quality degradation, and increased production costs. These outbreaks disrupt supply chains and may slow the industry's projected growth of 5−8% annually, underscoring the urgent need for innovative, sustainable disease management strategies.[8] Therefore, it is crucial to focus on developing and implementing more affordable techniques to manage bacterial blight effectively.[9−11] Besides, metal nanoparticles (NPs), such as copper (Cu) NPs,[12−14] silver (Ag) NPs,[15] gold (Au) NPs,[16,17] titanium dioxide (TiO_2) NPs,[18] and hybrid NPs[18] offer a novel and eco-friendly approach for treating bacterial diseases in plants due to their low toxicity, high fertility, and antibacterial properties.[19,20] Especially, Cu NPs exert antibacterial activities for different bacteria species including plant pathogens.[21] Cu NPs penetrate bacterial cells then initiate a cascade of events, leading to bacterial cell death through generation of reactive oxygen species (ROS) within the bacterial cell.[22,23] Additionally, Cu NPs can disrupt bacterial DNA replication and adenosine triphosphate (ATP) production.[24] However, production of Cu NPs using chemical methods is expensive and those NPs are phytotoxic at higher concentrations.[2,25] Even though, Cu NPs synthesized via green methods are mostly cost-effective and not phytotoxic.[26−30]

Received: January 11, 2026
Revised: April 6, 2026
Accepted: April 14, 2026
Published: April 18, 2026

On the other hand, *Anthurium andraeanum*, a tropical ornamental plant from the *Araceae* family, a diverse group with over 100 genera and 1500 species, is a key player in the global cut flower industry.[31,32] However, its cultivation is severely threatened by bacterial blight caused by *Xanthomonas axonopodis pv. dieffenbachiae* (XAD), which can lead to devastating crop losses of up to 100% in newly affected regions.[33−35] The disease is notoriously difficult to manage once introduced, and most anthurium varieties are highly susceptible.[33,34]

This study presents a cost-effective, sustainable strategy for managing bacterial blight by leveraging nanobiotechnology, anchored in the principles of chemistry as the central science connecting chemical biology, materials science, and environmental sustainability. Cu NPs were synthesized via chemical, semichemical, and green approaches, the latter innovatively utilizing leaf extracts from the host plant itself and characterized through advanced material characterization techniques. *In vitro* and *in vivo* evaluations demonstrated potent antibacterial activity against *Xanthomonas* sp., with complete disease remission in 90% of treated *A. andraeanum* plants and no observed phytotoxicity. To the best of our knowledge, this study represents the first demonstration of Cu NPs mediated control of bacterial blight specifically in *A. andraeanum*, offering a promising alternative to conventional treatments in floriculture disease management. By integrating synthetic chemistry, green nanotechnology, and applied plant science, this research underscores how chemical innovation can drive sustainable solutions in agriculture and floriculture.

2. EXPERIMENTAL METHODS

Cu NPs were synthesized using three distinct approaches: (1) chemical reduction, (2) semichemical reduction, and (3) green synthesis. In the chemical reduction, copper chloride ($CuCl_2$) was used as the precursor, sodium hydroxide (NaOH) served as the reducing agent, and polyvinylpyrrolidone (PVP) acted as the stabilizer during the controlled precipitation process. In the semichemical reduction, $CuCl_2$ was again the precursor, citrus juice provided natural reducing agents (biomolecules such as flavonoids and organic acids), and NaOH was used to adjust pH, enabling precipitation. In the green synthesis method, $CuCl_2$ was the precursor, anthurium leaf extract supplied phytochemicals as the reducing agent, and the process relied on biomediated precipitation without additional synthetic stabilizers. Detailed synthesis procedures are provided in Section 1 of the Supporting Information, with schematic representations shown in Figure S1a−c. The composition of the green synthesis medium is summarized in Table S1, while phytochemical screening results and corresponding interpretations for the plant extract are presented in Table S2. The structural and physicochemical properties of the synthesized Cu NPs including bulk structure, nanostructure, surface morphology, particle size, crystalline phase, and chemical functionality were characterized by using powder X-ray diffraction (PXRD), high-resolution transmission electron microscopy (HRTEM), selected area electron diffraction (SAED), scanning electron microscopy (SEM), particle size analysis via dynamic light scattering (PSA-DLS), and attenuated total reflection Fourier-transform infrared spectroscopy (ATR FTIR). PXRD was performed using a Bruker D8 diffractometer with Cu Kα radiation (λ = 1.5406 Å) over a 2θ range of 5−80° to determine the crystalline phase and structure. HRTEM analysis was carried out on a JEOL JEM-2100 microscope at 200 kV, with samples prepared by dispersing nanoparticles in water and drop-casting onto carbon-coated copper grids. SEM imaging was done using a Hitachi SU6600 FE-SEM at 10 kV, with samples mounted on stubs and sputter-coated with gold to enhance the conductivity. For the bactericidal effects, cells were fixed using glutaraldehyde, dehydrated through graded ethanol, critical-point dried, sputter-coated with Au, and imaged at 200 kV; representative fields (≥5 per condition) were captured at a 2−5 μm scale. ATR-FTIR analysis was performed using an ABBMB 3000 FTIR spectrometer (Switzerland) to investigate the surface chemistry and functional groups of the synthesized Cu NCs. Spectra were recorded between 475−4000 cm^{-1} at a resolution of 8 cm^{-1}, with 64 consecutive scans, and each measurement was conducted in triplicate to ensure reproducibility. Additionally, SAED patterns were recorded to confirm crystallinity and phase identification (please refer to Section 3 under Supporting Information for more experimental details).

The antibacterial performance of Cu NPs was evaluated through both *in vitro* and *in vivo* assays (please refer to Sections 4−8 in Supporting Information). First, the leaves of *A. andraeanum* showing bacterial blight symptoms were collected. The leaves were ground into a fine paste, and the extract was prepared. A 10-fold diluted extract was inoculated onto Luria-Bertani (LB) medium. After 3 days, well-developed yellow bacterial colonies were observed and subsequently subcultured on fresh LB medium. Gram staining and pathogenicity tests were performed to confirm bacterial identity. The antibacterial activity of the synthesized Cu NPs was quantified using minimum inhibitory concentration (MIC) and minimum bactericidal concentration (MBC) assays against *Xanthomonas* spp. Bacteria isolated from infected anthurium leaves were cultured in LB broth (1×10^6 CFU/mL). Serial 2-fold dilutions of Cu NP samples (500−0.9 μg/mL) were prepared and incubated with the bacterial suspension in 96-well plates at 37 °C for 24 h. MIC was determined by measuring OD_{600} to identify the lowest concentration inhibiting visible growth. For MBC, aliquots from nonturbid wells were plated on LB agar and incubated for 72 h to identify the lowest concentration that produced no bacterial colonies. These assays enabled quantitative comparison of the antibacterial potency of Cu NPs synthesized by methods A, B, and C. For the *in vitro* study, a well-diffusion method was employed to assess the activity against *Xanthomonas* sp. In the well-diffusion test, the bacterial cultures were treated with Cu NPs synthesized by three different methods, at concentrations of 30, 50, and 100 ppm. The *in vivo* experiment involved 129 anthurium plants inoculated with the pathogen, followed by treatment with Cu NPs (50−200 ppm) after disease establishment (please refer Figure S13: copper nano clusters treatment plan to *A. andraeanum* plants for a more detailed understanding). Disease progression was monitored over 12 weeks by measuring lesion areas, and statistical significance of treatments was determined using two-way analysis of variance (ANOVA). The authors confirm that all methods were performed following the relevant guidelines and regulations.[36]

3. RESULTS AND DISCUSSION

The Cu NPs synthesized via three methods displayed distinct visual and structural characteristics. Method A (chemical reduction at pH 12, ∼70 °C) produced zinnwaldite brown Cu NPs [Figure S3a], method B (semichemical reduction at pH 12, ∼70 °C) yielded smoky black particles [Figure S3b], and method C (green synthesis at pH 10, ∼70 °C) resulted in Pullman brown particles [Figure S3c]. PXRD analysis [Figure 1a] confirmed that each method produced unique crystalline phases and microstructures, with all samples showing an amorphous hump between 10 and 22° due to capping agents. Method A exhibited sharp peaks at 35.50, 38.70, 48.70, 53.40, 58.30, 61.50, 66.20, and 74°, corresponding to CuO and Cu planes (JCPDS No. 00-001-1548), indicating a face-centered cubic (fcc) copper structure.[37] Method B showed peaks at 29.60, 35.80, and 43.00°, assigned to Cu_2O planes (JCPDS No. 00-005-0667), confirming fcc Cu_2O crystallinity. Method C displayed seven distinct peaks at 29.00, 34.50, 38.90, 42.30, 43.80, 48.40, and 58.30°, corresponding to Cu_2O, CuO, and Cu planes (JCPDS Nos. 00-001-1548, 00-005-0667, 00-004-0836), highlighting the mixed-phase nature of green-synthesized Cu NPs.[38,39] A semiquantitative reference intensity ratio

https://doi.org/10.1021/acsomega.6c00344
ACS Omega 2026, 11, 25657−25665

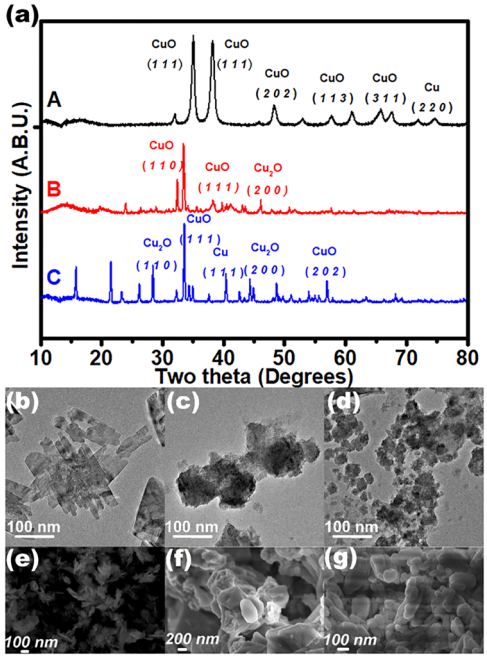

Figure 1. (a) PXRD profiles of Cu NPs synthesized via chemical, semichemical, and green approaches. HRTEM images of Cu NPs obtained via (b) chemical reduction-A, (c) semichemical reduction-B, (d) green synthesis-C; SEM images of Cu NPs produced via (e) chemical reduction, (f) semichemical reduction, (g) green synthesis approaches.

[RIR (I/I_c)] analysis was carried out with the aid of DIFFRAC.EVA (Bruker) on nonoverlapping reflections Cu_2O (1 1 0/2 0 0), CuO ($\bar{2}$ 0 2/ 2 0 2), Cu (2 0 0/2 2 0), and normalized within the CuO−Cu_2O−Cu subset to reveal the dominant phases in each method.[40] The resulting fractions demonstrate that method A is CuO-rich (∼86% CuO, ∼4% Cu_2O, ∼10% Cu), whereas method B and method C are Cu_2O-rich (∼67% Cu_2O, ∼33% CuO/∼48% Cu_2O, ∼31% CuO, ∼21% Cu, respectively). These values substantiate that Cu_2O is the predominant crystalline oxide in method B and method C (with CuO), while CuO predominates in method A (please refer to Table S3 available in Supporting Information for more details). The results obtained for FTIR further supported these claims (Figure S4). Method A-derived Cu NPs exhibit strong C═O and N−H bending peaks indicating PVP residues from chemical precursors. Cu NPs produced via method B dominated by the Cu_2O peak at 615 cm^{-1} with minimal organic functional groups. Cu NPs from method C showed N−H and C−N peaks (plant biomolecules) [please refer to the Section 2 in Supporting Information for the detailed phytochemical analysis], along with CuO and Cu_2O peaks, confirming bioreduction and capping. These NPs' morphological shapes derived from three different synthesis methods were identified as flower petal/plate shaped, polyhedral shaped and rod-shaped NPs according to their synthesis methods, respectively. Table S4 summarizes the identified morphological features including crystalline phases, surface functionality, and average diameters of the particles.

Besides, the nanostructures of the materials can be seen in Figure 1b−d. All the captured HRTEM images clearly showed that the Cu derived NPs exist in agglomerate form. Furthermore, the marked boundaries of the NPs can be seen in Figure S5. Moreover, the SEM images captured further supported this evidence, as shown in Figure 1e−g.

The agglomeration of NPs is responsible for the formation of these aggregated Cu NPs. In general, agglomeration can take place at two distinct stages: primary agglomeration, which occurs during the precipitation process, and secondary agglomeration, which arises during the drying phase. Primary agglomeration happens because particles collide and stick together while they are forming in solution, a process known as Smoluchowski ripening.[41] Secondary agglomeration, on the other hand, is due to Ostwald ripening, where smaller particles tend to merge into larger ones during drying to reduce their surface energy.[41]

Particle size refers to the overall dimensions of a particle, which may consist of several smaller crystalline regions called crystallites. According to PSA, it was identified that particle size derived from method A is between 10 and 200 nm range, while Cu NPs from method B are between 20 and 500 nm. Cu NPs formed via green synthesis demonstrated a particle size in the range of 30−250 nm. This is reasonable, as PSA tends to report larger sizes because it measures particles in their hydrated or agglomerated state, includes surrounding solvent layers, and assumes spherical geometry.[41] (The relevant particle size distribution histograms can be seen in Figure S6.) In contrast, SEM and HRTEM provide direct high-resolution images of the actual particle dimensions. Further to that, the crystallite sizes of the Cu NPs were determined from PXRD analysis using both the Debye−Scherrer equation and the Williamson−Hall (W−H) model (please refer to Section 3.2 in Supporting Information), revealing significant insights into their microstructure.[18] For method A (86% CuO dominant), both methods gave similar sizes (∼9−11 nm), indicating minimal strain. For method B (67% Cu_2O dominant), a significant discrepancy was observed: the Scherrer average was ∼13.4 nm, but the W−H model calculated a larger size of ∼19.1 nm with 0.20% tensile strain. This shows the Scherrer method underestimated the size by not accounting for strain, and the anisotropic peak broadening suggests possible nonspherical particle shapes. For method C [mixed phases: CuO (31%), Cu_2O (48%), and Cu (21%)], analysis of the CuO phase showed a similar trend. The Scherrer average was ∼14.6 nm, whereas the W−H model resulted in ∼23.9 nm with 0.06% tensile strain. The associated metal Cu particles were estimated at ∼10.3 nm via the Scherrer equation.

In addition, the SAED patterns shown in Figure S7a−c further confirm the polycrystalline nature and phase purity, showing rings consistent with the material structure, which aligns perfectly with the PXRD results.[42] The identified phases further confirmed that method A-derived Cu NPs have CuO-dominant phases [(1 1 1), (2 0 0), (2 2 0), and (4 0 0)]. Cu NPs synthesized from a semichemical approach (method B) yielded three identified phases relevant to Cu_2O [(1 1 1), (2 0 0), (2 2 0)]. The Cu NPs synthesized via method C (green approach) contained mixed phases [Cu_2O: (1 1 1), (2 2 0); CuO: (4 0 0); Cu (2 0 0)]. Further, the SAED pattern radii provide a complementary, localized perspective that aligns with the bulk-average PXRD data. The radii for method A (2.3−14.3 nm) fall within a range that brackets the XRD crystallite sizes (∼9−11.0 nm), confirming a uniform population of CuO-dominant nanoparticles. For method B, the broad distribution of SAED radii (2−8.05 nm) strongly justifies the appearance of significant anisotropy and nonspherical

https://doi.org/10.1021/acsomega.6c00344
ACS Omega 2026, 11, 25657−25665

morphologies like polyhedron, as the measured radius in a two-dimensional (2D) projection can vary dramatically with particle orientation. The SAED results for method C (2.34−9.84 nm) show another widest distribution, which directly validates the multiphase nature of the sample; the smallest radii correspond well to the metallic Cu nanoparticles (~10 nm), while the larger values are consistent with the presence of the larger CuO and Cu_2O crystallites identified by PXRD.

The general agreement between the techniques confirms the overall size regimes and phases, while the expected discrepancies highlight the fundamental difference between a bulk-average crystallite size (PXRD) and the visual size distribution of individual particles (SAED).[42]

The antibacterial efficacy of Cu NPs synthesized via chemical reduction (A), semichemical reduction (B), and green synthesis using Anthurium leaf extract (C) was evaluated against *Xanthomonas* sp., both *in vitro* and *in vivo* on infected Anthurium plants. (Detailed experimental steps involved in isolation of *Xanthomonas* bacteria, culture media preparation, inoculation, subculturing, gram staining, pathogenicity test, minimum inhibitory concentration (MIC)/minimum bactericidal concentration (MBC) assays, well-diffusion method, antibacterial property evaluation test of Cu NPs at *in vivo* level, two-way ANOVA analysis were summarized under Sections 4−11 in Supporting Information.) As shown in Figure S10-the (MIC) and Figure S11-(MBC) assays were conducted to quantify antibacterial potency accurately in order to validate whether the synthesized Cu NPs exhibit true inhibitory or bactericidal effects before further comparative analysis.[43] Table 1 summarizes the MIC/MBC values of synthesized Cu NPs via methods A, B, and C.

Table 1. Summary of the MIC and MBC Assay Results

sample	MIC (μg/mL)	MBC (μg/mL)	description
A	31.25	62.50	MIC and MBC are close bactericidal tendency
B	62.50	125	MIC and MBC are close to bactericidal tendency. Requires a higher concentration to achieve a bactericidal effect
C	31.25	62.50	MIC and MBC are close bactericidal tendency
+ control	15.62	31.25	confirms assay validity

Based on the results, it can be understood that the synthesis route had a clear influence on the antibacterial performance of the Cu NPs. NPs produced via methods A and C demonstrated the highest potency, exhibiting the lowest MIC values (31.25 μg/mL) and achieving complete bacterial inactivation at 62.50 μg/mL. In contrast, method B produced comparatively weaker NPs, requiring 62.50 μg/mL to inhibit growth and a higher concentration of 125 μg/mL to achieve a bactericidal effect.

These quantitative MIC/MBC trends are consistent with the *in vitro* well-diffusion results. At 30 ppm, Cu NPs synthesized via methods A, B, and C produced inhibition zones of 25 ± 0.81, 15 ± 0.81, and 20.6 ± 0.94 mm, respectively; further confirming that methods A and C yield more active antibacterial formulations than method B. The antibiotic sulfamethoxazole generated a slightly larger zone (26.3 ± 0.47 mm), validating the assay's reliability. As expected, the negative control (distilled water) produced no inhibition, with *Xanthomonas* sp. freely growing around the wells, indicating that all observed effects were attributable to the NPs treatments [Figure 2a,b].

In contrast, the *in vivo* results (Table 2) show that synthesis method C (green synthesis) performs best overall, achieving 90% disease control even at the lowest concentration (50 ppm), although it takes slightly longer than chemical synthesis at higher doses. Method A (chemical synthesis) becomes highly effective at higher concentrations (100−200 ppm), showing faster action compared with the other methods. Besides, method B (semichemical synthesis) is the least effective, requiring higher concentrations and longer exposure times to reach comparable control levels. Overall, the data indicate that method C is the most efficient at low doses, while method A delivers the fastest suppression at higher concentrations. A summary of the performance of Cu NPs under *in vivo* conditions can be seen in Table 2.

To further claim this, the direct evidence of the bactericidal tendency of the synthesized Cu NPs at their optimized concentrations was captured via SEM. The SEM micrographs reveal distinct morphological alterations in *Xanthomonas* cells following exposure to Cu NPs synthesized via methods A, B, and C as shown in Figure 2c−f. As visualized in Figure 2c, the untreated *Xanthomonas* cells exhibit the typical smooth, rod-shaped morphology with intact, well-defined cell walls, indicating healthy, uncompromised cells. The cells treated with Cu NPs synthesized by method A [Figure 2d] show noticeable deformation and collapse of the bacterial envelope. The previously smooth surfaces become wrinkled and irregular, suggesting membrane disruption and loss of structural integrity, which aligns with the strong MIC/MBC results obtained for method A. In parallel, method B NP-treated cells showed moderate structural damage, with partial surface roughening and deformation. The degree of distortion is less severe than methods A and C, consistent with the higher MIC/MBC values and lower antibacterial potency observed for method B. Cells exposed to method C Cu NPs displayed an extensive disintegration, with many cells appearing collapsed, fragmented, or embedded in aggregated debris. This severe distortion reflects a strong bactericidal effect, supporting both the MIC/MBC data and the effectiveness *in vivo* performance observed for method C. Besides, the positive control (sulfamethoxazole) showed only moderate, nonlasting control (30% within 2 weeks, with symptom return), and its use at high concentrations (>150 ppm) was avoided due to potential phytotoxicity.[44,45] It may inhibit plant growth, affect photosynthesis, and disrupt nutrient uptake. Also, it may persist in the environment, potentially contaminating soil and water.[46,47] The negative control (distilled water) resulted in disease progression.

In addition to that, a two-way analysis of variance (ANOVA) was conducted to evaluate the effects of the synthesis method and Cu NP concentration on the control of bacterial blight in anthurium. Treatment method [chemical reduction (A), semichemical reduction (B), and green synthesis (C)] and Cu NP concentration (50, 100, and 200 ppm) were specified as independent categorical variables, with mean lesion diameter (mm) serving as the continuous dependent variable. The analysis was performed using Origin Pro 2018, with a significance threshold of $\alpha = 0.05$ for all tests. Table 3 summarizes the main effects and interactions of the two-way ANOVA.

https://doi.org/10.1021/acsomega.6c00344
ACS Omega 2026, 11, 25657−25665

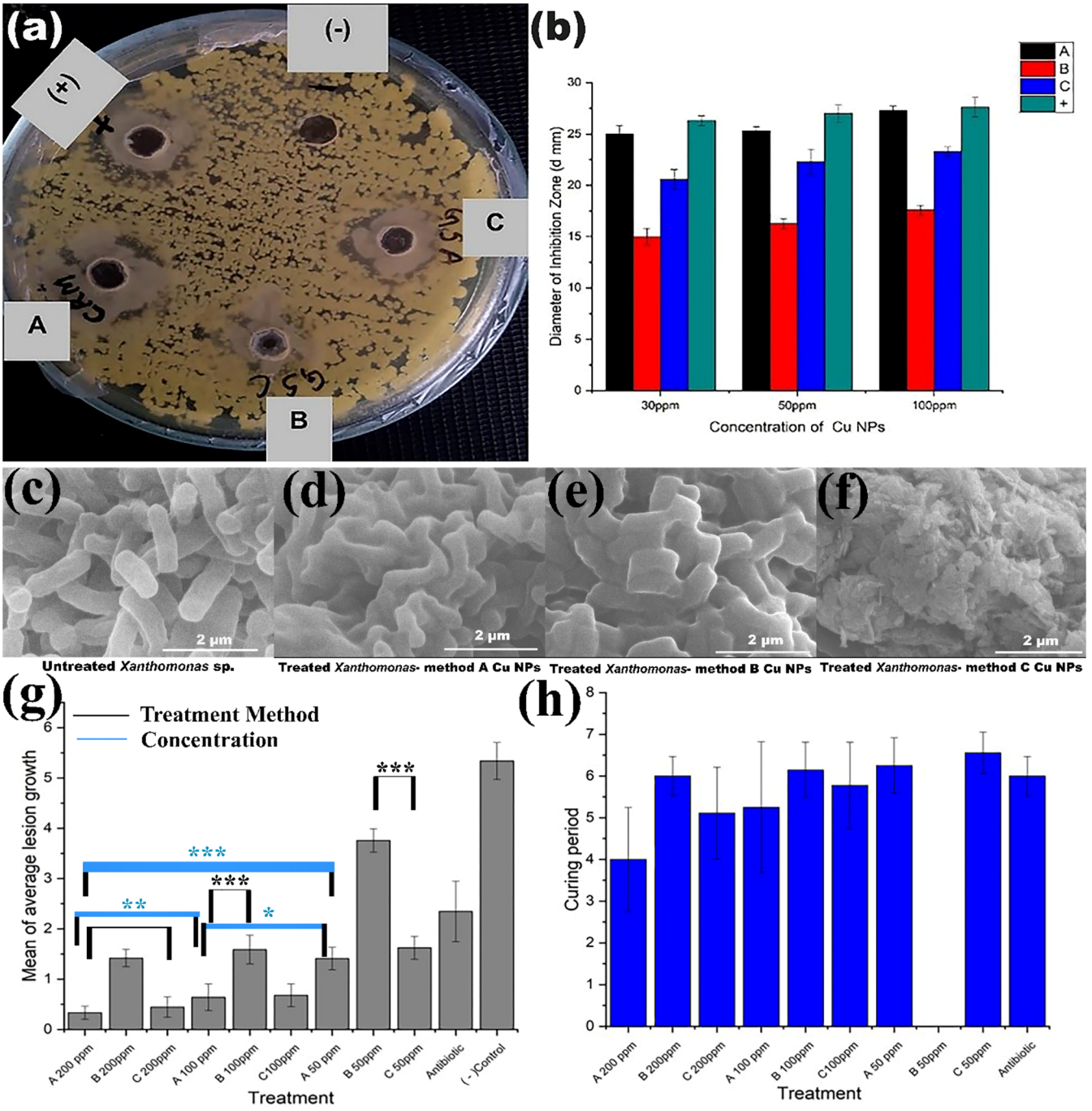

Figure 2. (a) Antibacterial activity of Cu NPs in the well-diffusion method: Inhibition zoned formed around the well filled with Cu NPs synthesized by methods A, B, C, (+) control-antibiotic sulfamethoxazole and (−) control-distilled water and (b) a bar graph of the antibacterial properties of Cu NPs synthesized by methods A, B, C, (+) control-antibiotic sulfamethoxazole under *in vitro* conditions. A SEM micrograph of (c) untreated *Xanthomonas* sp., (d) bactericidal effect from method A-derived Cu NPs, (e) bactericidal effect from method B-derived Cu NPs, (f) SEM capture of bactericidal effect from method C-derived Cu NPs, (g) means of average lesion growth of plants treated with different concentrations of Cu NPs synthesized via method A, method B, and method C, and (h) means of curing period (weeks) of plants treated with different concentrations of Cu NPs synthesized via method A, method B, and method C [(*, **, ***) denote significance at $p < 0.05$, $p < 0.01$, and $p < 0.001$, respectively].

Table 2. Summary of Performance of Cu NPs under *In Vivo* Conditions

synthesis method	50 ppm (90% control)	100 ppm (90% control)	200 ppm (90% control)	key observation
chemical (A)	80% control in 6 weeks	90% control in 5 weeks	90% control in 4 weeks	effective at high concentration
semichemical (B)	no control	80% control in 6 weeks	90% control in 7 weeks	least effective, slowest action
green (C)	90% control in 7 weeks	90% control in 6 weeks	90% control in 5 weeks	most effective at low concentrations

https://doi.org/10.1021/acsomega.6c00344
ACS Omega 2026, 11, 25657−25665

Table 3. Statistical Significance of the Main Effects for Both Independent Variables in a Two-Way ANOVA

factor	degrees of freedom	*F*-statistic	*p*-value	interpretation
treatment method	(2, 18)	34.27	<0.001	highly significant; lesion diameter differs substantially by synthesis route
concentration	(2, 18)	28.54	<0.001	highly significant; clear dose-dependent response observed
treatment concentration	(4, 18)	1.23	0.332	not significant; effects of treatment and concentration are independent (biological meaning: the effect of treatment method does not depend on the concentration used; the relative efficacy of the three synthesis methods remains consistent across all three concentration levels. Similarly, the dose−response relationship (higher concentration = better control) holds true regardless of which treatment method is used)

To identify specific differences between groups, Tukey's honestly significant difference (HSD) post hoc test was applied following the ANOVA.

As displayed in Table S16, both the chemically reduced (A) and green-synthesized (C) Cu NPs demonstrated significantly superior disease suppression compared to the semichemical route (B), with mean lesion diameters reduced by approximately 4 mm ($p < 0.001$ for both). However, no statistically significant difference was detected between treatments A and C ($p = 0.214$), indicating that the chemical and green synthesis methods yield comparable *in vivo* antibacterial efficacy under the tested conditions. In addition to that, a comparison between each concentration was made, as can be seen in Table S17.

As Table S17 summarizes, a clear dose-dependent relationship was observed. The 50-ppm treatment resulted in significantly larger lesion diameters than both 100 ppm ($p < 0.05$) and 200 ppm ($p < 0.001$), confirming that this concentration is insufficient for rapid disease control. Furthermore, 200 ppm significantly outperformed 100 ppm ($p < 0.01$), establishing 200 ppm as the most effective concentration evaluated.

These statistical findings directly validate the empirical observations presented in Figure 2g,h. The superior efficacy of treatments A and C at 100 and 200 ppm correlates precisely with their rapid suppression of sp. proliferation and the correspondingly low mean lesion diameters recorded over the 12-week monitoring period. In contrast, the significantly poorer performance of treatment B across all concentrations reflects its slower antibacterial action, resulting in a prolonged disease progression and larger lesion areas.

The dose-dependent effect confirmed by post-hoc analysis aligns with the observed curing timelines, i.e., plants treated with 200 ppm exhibited lesion arrest within 3−4 weeks, while those receiving 50 ppm required extended periods (7−9 weeks) to achieve comparable disease control, with some individuals showing incomplete recovery. This concentration-dependent response underscores the critical importance of optimizing the Cu NP dosage for practical field applications.

In contrast, the observed antimicrobial efficacy of the NPs can be rationalized by considering several interrelated physicochemical factors, including electronegativity and membrane interactions, oxidation state-dependent redox activity, effective charge-to-radius (e/r) ratio, and subsequent bioactivity.[48−51] The effective ionic charge plays a critical role in governing interactions with the bacterial membrane. Notably, CuO NPs possess a higher charge density and greater electronegativity than Cu_2O NPs, which enhances their electrostatic attraction to the negatively charged phospholipid head groups and teichoic acids present on the Gram-negative *Xanthomonas* cell envelope (Figure S5). This stronger interfacial adhesion facilitates more pronounced membrane destabilization, lipid peroxidation, and cellular uptake, collectively contributing to the superior antibacterial performance observed for CuO-dominant NPs.[52]

In addition, the higher e/r ratio of CuO NPs enables strong coordination with sulfur- and nitrogen-containing functional groups in essential bacterial enzymes, including those involved in dehydrogenase activity and respiratory electron transport chains.[48] Such tightly bound interactions can induce enzyme denaturation, disrupt metabolic pathways, and ultimately lead to rapid bacterial inactivation. Although Cu_2O NPs also interact with similar biomolecular targets preferentially binding to sulfur-containing cysteine residues, their comparatively lower e/r ratio results in weaker binding kinetics and reduced affinity. This illustrates a less immediate metabolic shutdown and a diminished antimicrobial response relative to CuO NPs.[48]

The oxidation state of copper further governs the antibacterial performance through redox-driven mechanisms. Cu(II), predominant in CuO NPs (method A), exhibits a higher redox potential and acts as a stronger oxidizing agent than Cu(I) present in Cu_2O NPs (method B). This enhances the potential catalytic generation of reactive oxygenated species (ROS), including hydroxyl radicals (*OH), via Fenton-like and Haber−Weiss reactions.[51−53] The resulting rapid and intense ROS burst possibly causes extensive oxidative damage to bacterial membranes, proteins, and nucleic acids, explaining the shortest disease control period observed (4 weeks). In contrast, Cu(I) species exhibit lower oxidative potency, and their antibacterial action likely depends on gradual oxidation to Cu(II) on the bacterial surface or within the cell. This process possibly generates ROS more slowly, yielding a sustained but delayed antibacterial effect that correlates with the longest treatment duration (7 weeks). Green-synthesized mixed-phase Cu NPs containing Cu^0, Cu^+, and Cu^{2+} species demonstrate a synergistic antibacterial mechanism. Metallic copper (Cu^0) NPs act as a redox reservoir that undergoes progressive oxidation, enabling the sustained release of Cu^+ and Cu^{2+} ions. This multivalent system probably combines rapid ROS-mediated damage driven by Cu^{2+} with a prolonged ion-mediated membrane and enzymatic disruption arising from Cu^0/Cu^+. Consequently, this synergistic, multipronged mode of action results in highly effective antibacterial performance with an intermediate disease control period of approximately 5 weeks.

Additionally, plants treated with Cu NPs exhibited no signs of phytotoxicity throughout the 12-week observation period. After 7 weeks, bacterial blight symptoms caused by *Xanthomonas* sp. were completely absent and plants continued to grow healthy during the remaining weeks.

https://doi.org/10.1021/acsomega.6c00344
ACS Omega 2026, 11, 25657−25665

4. CONCLUSIONS

The antibacterial efficacy of the synthesized Cu-based NPs is strongly shaped by the synthesis route, which governs their morphology, particle size, crystallographic phases, surface chemistry, and dispersion stability. These physicochemical characteristics directly influence Cu^{+}/Cu^{2+} ion-release behavior, surface reactivity, and NP−cell interactions, thereby determining the antibacterial performance across both *in vitro* and *in vivo* conditions.

Quantitative MIC and MBC measurements confirmed that nanoparticles produced via methods A and C possess the highest inherent antibacterial potency (MIC = 31.25 μg/mL; MBC = 62.50 μg/mL), while method B exhibited lower activity. This ranking was consistent with the well-diffusion assay at 30 ppm (A > C > B), reflecting both intrinsic antibacterial strength and differences in NP diffusion and aggregation in solid media. SEM imaging further validated these findings, revealing progressive membrane deformation, collapse, and fragmentation in *Xanthomonas* sp. cells following exposure to the NPs.

The differences in antibacterial kinetics among the three methods can be attributed to their distinct phase compositions and oxidation states. Method A produced CuO-rich (86%) NPs, which acted rapidly due to the high oxidative reactivity of Cu^{2+} species. Methods B and C yielded Cu_2O-rich systems (67 and 48%, respectively) that exerted more gradual antibacterial effects, consistent with sustained Cu^{+} release and moderated reactivity. Mixed-phase NPs combined features of both oxidation states, enabling complementary and potentially synergistic antibacterial mechanisms.

The green-synthesized nanoparticles from method C, comprising rod-shaped $Cu/Cu_2O/CuO$ structures stabilized by plant-derived capping agents, demonstrated excellent dispersion stability, enhanced adhesion to leaf surfaces, and controlled ion release. These attributes enabled highly effective disease suppression *in vivo*, achieving 90% control at only 50 ppm and strong long-term protection. In comparison, the chemically and semichemically synthesized NPs (methods A and B) required higher dosages to deliver similar outcomes. Importantly, all treated plants remained free of bacterial blight symptoms and exhibited no phytotoxicity over a 12-week period, confirming the safety and practical applicability of these materials.

Overall, this study establishes that the synthesis-dependent modulation of NP morphology, phase composition, and surface chemistry is central to optimizing antibacterial activity. These structure−function relationships link the observed MIC/MBC values to zone-of-inhibition patterns and, ultimately, to successful *in vivo* disease control. While the antibacterial effects are clearly demonstrated, the underlying molecular mechanisms, particularly the role of ROS, require further experimental validation. Future work will include ROS-specific assays (e.g., DCFH-DA assay) and ion-release profiling to clarify the interplay between ionic and particulate pathways. In the present work, our primary aim was to investigate the applicability of the synthesized Cu NPs for mitigating bacterial blight disease in Anthurium using three complementary approaches, and the findings provide compelling evidence supporting their viability as a next-generation antibacterial strategy.

■ ASSOCIATED CONTENT

Supporting Information

The Supporting Information is available free of charge at https://pubs.acs.org/doi/10.1021/acsomega.6c00344.

Comprehensive supporting data and analyses for the study on Cu-based nanoparticles (Cu NPs) and their antibacterial efficacy against *Xanthomonas* sp. It includes: Sections 1−3: Detailed synthesis protocols, phytochemical profiling, and advanced characterization (SEM, TEM, PXRD, FTIR, PSA) of Cu NPs; Sections 4−8: *In vitro* antibacterial evaluations, including Gram staining, pathogenicity confirmation, and MIC/MBC/well-diffusion assays; Sections 9 and 10: *In vivo* application results on Anthurium plants, highlighting disease suppression and phytotoxicity assessment over 12 weeks; Section 11: Statistical validation using two-way ANOVA; Section 12: Tukey's honestly significant difference (HSD) post-hoc test; the supporting file features Figures S1−S16 and Tables S1−S17, illustrating synthesis pathways, morphological differences, antibacterial performance, and statistical outcomes for clarity and reproducibility (PDF)

■ AUTHOR INFORMATION

Corresponding Author

Colin N. Peiris − *Department of Applied Sciences, Sri Lanka Institute of Information Technology, 10115 Malabe, Colombo, Sri Lanka*; Email: colin.p@sliit.lk

Authors

Sanka Wanaguru − *Department of Applied Sciences, Sri Lanka Institute of Information Technology, 10115 Malabe, Colombo, Sri Lanka*

Sehan Jayasinghe − *Department of Applied Sciences, Sri Lanka Institute of Information Technology, 10115 Malabe, Colombo, Sri Lanka;* orcid.org/0009-0005-1769-8710

Kasun Seneviratne − *Ministry of Irrigation and Water Resources Management, 01000 Colombo, Sri Lanka*

Nilwala Kottegoda − *Department of Chemistry, University of Sri Jayewardenepura, 10250 Colombo, Sri Lanka;* orcid.org/0000-0002-9664-1704

Sriyani E. Peiris − *Department of Applied Sciences, Sri Lanka Institute of Information Technology, 10115 Malabe, Colombo, Sri Lanka*

Complete contact information is available at: https://pubs.acs.org/10.1021/acsomega.6c00344

Author Contributions

The grant application was overseen by Prof. S.E.P. as the Principal Investigator. Further, Prof C.N.P., Prof. S.E.P., Prof N.K., S.J., and K.S. contributed to conceptualization of the project. All the formal analysis was performed by S.W. and S.J.; S.W. wrote the first draft of the manuscript. All other authors contributed equally to revising and improving the definitive version of the manuscript.

Notes

We hereby declare that, to the best of our knowledge, this submission is our original work. It does not contain any material previously published or written by another person, nor does it include substantial material that has been accepted for

https://doi.org/10.1021/acsomega.6c00344
ACS Omega 2026, 11, 25657−25665

the award of any other academic qualification at any university or other institute of higher learning, except where proper acknowledgment is made in the text.
The authors declare no competing financial interest.

■ ACKNOWLEDGMENTS

The authors gratefully acknowledge the financial support provided by Sri Lanka Institute of Information Technology (SLIIT) (Grant No: PVC(R&I)/RG/2023/01). Moreover, research facilities of the Department of Applied Sciences of SLIIT are appreciated, and the authors extend their appreciation to Sri Lanka Institute of Nano Technology and Institute of Chemistry Ceylon for facilitating advanced analytical instruments.

■ REFERENCES

(1) Din, B. N. M.; Ali, N. S.; Tan, G. H.; Yusop, M. R. Current Status of Bacterial Leaf Blight in Malaysian Rice Plants. *J. Curr. Opin. Crop Sci.* **2023**, *4* (1), 1−12.
(2) Mondal, K. K.; Mani, C. Investigation of the Antibacterial Properties of Nanocopper against Xanthomonas axonopodis pv. punicae, the Incitant of Pomegranate Bacterial Blight. *Ann. Microbiol.* **2012**, *62* (2), 889−893.
(3) Sharma, J.; Sharma, K. K.; Kumar, A.; Mondal, K. K.; Thalor, S.; Maity, A.; Jadhav, V. T. Pomegranate Bacterial Blight: Symptomatology and Rapid Inoculation Technique for Xanthomonas axonopodis pv. punicae. *J. Plant Pathol.* **2017**, *99*, 109−119.
(4) Ntasiou, P.; Kaldeli Kerou, A.; Karamanidou, T.; Vlachou, A.; Tziros, G. T.; Tsouknidas, A.; Karaoglanidis, G. S. Synthesis and Characterization of Novel Copper Nanoparticles for the Control of Leaf Spot and Anthracnose Diseases of Olive. *Nanomaterials* **2021**, *11* (7), 1667.
(5) Devadath, S. In *Chemical Control of Bacterial Blight of Rice*, International Workshop on Bacterial Blight of Rice, 1989; pp 89−98.
(6) Pandit, M. A.; Kumar, J.; Gulati, S.; Bhandari, N.; Mehta, P.; Katyal, R.; Kaur, J.; et al. Major Biological Control Strategies for Plant Pathogens. *Pathogens* **2022**, *11* (2), 273.
(7) Rizzo, D. M.; Lichtveld, M.; Mazet, J. A.; Togami, E.; Miller, S. A. Plant Health and Its Effects on Food Safety and Security in a One Health Framework: Four Case Studies. *One Health Outlook* **2021**, *3* (1), No. 6.
(8) Global Market Insights. Floriculture Market Size, Share and Industry Analysis Report. https://www.gminsights.com/industry-analysis/floriculture-market (accessed Sept 25, 2025).
(9) Chen, F. C. Genetic Engineering of Anthurium for Bacterial Disease Resistance. Ph.D. Dissertation, University of Hawai'i at Manoa, 1993.
(10) Oliva, R.; Ji, C.; Atienza-Grande, G.; Huguet-Tapia, J. C.; Perez-Quintero, A.; Li, T.; Eom, J.-S.; et al. Broad-Spectrum Resistance to Bacterial Blight in Rice Using Genome Editing. *Nat. Biotechnol.* **2019**, *37* (11), 1344−1350.
(11) Ranjani, P.; Gowthami, Y.; Gnanamanickam, S. S.; Palani, P. Bacteriophages: A New Weapon for the Control of Bacterial Blight Disease in Rice Caused by Xanthomonas oryzae. *Microbiol. Biotechnol. Lett.* **2018**, *46* (4), 346−359.
(12) Chatterjee, A. K.; Chakraborty, R.; Basu, T. Mechanism of Antibacterial Activity of Copper Nanoparticles. *Nanotechnology* **2014**, *25* (13), No. 135101.
(13) Peiris, S. E.; Seneviratne, K. L.; Shashikala, R. P. A.; Peiris, C. N.; Imalka, M. I.; Piumika, Y. P. *In Vitro* Evaluation of Antibacterial Activity of Copper and Sulfur Nanoparticles for Controlling Bacterial Blight Caused by *Xanthomonas* sp. in Anthurium andraeanum Lind. *SLIIT J. Humanit. Sci.* **2022**, *3* (1), 46 DOI: 10.4038/sjhs.v3i1.50.
(14) Wanaguru, S.; Peiris, C. N.; Peiris, S. E.; Jayasinghe, S. In *Green Synthesis, Characterization of Cu Nano Units and Evaluation of Antibacterial Properties towards the Bacterial Blight Control in Anthurium andraeanum Lind under In Vitro and In Vivo Conditions*, SLIIT International Conference on Advancements in Sciences and Humanities, 2024.
(15) Tan, K. S.; Cheong, K. Y. Advances of Ag, Cu, and Ag−Cu Alloy Nanoparticles Synthesized via Chemical Reduction Route. *J. Nanopart. Res.* **2013**, *15* (4), No. 1537.
(16) Das, A.; Dutta, P. Antifungal Activity of Biogenically Synthesized Silver and Gold Nanoparticles against Sheath Blight of Rice. *J. Nanosci. Nanotechnol.* **2021**, *21* (6), 3547−3555.
(17) Karuvelan, M.; Kaliyamoorthy, S.; Dhanaraj, S.; Chelliah, R.; Oh, D. H.Use of Gold Nanoparticles as a Nano-Weapon in Plant Disease Management. In *Plant Response to Gold Nanoparticles: Plant Growth, Development, Production, and Protection*; Springer, 2024; pp 271−310.
(18) Seneviratne, K. L.; Peiris, S. E.; Peiris, C. N.; Shashikala, R. P. A.; Jayasinghe, S.; Kottegoda, N. Facile Synthesis of Silver/Iron-TiO_2 Nanoparticles for Sterilization of Nodal Explants of Dracaena sanderiana Sander ex Mast. cvs 'Gold' and 'Victory' and Growth Regulator Effects on In Vitro Growth. *Iran. J. Catal.* **2025**, *15* (1), No. 152511, DOI: 10.57647/j.ijc.2025.1501.11.
(19) Bagherzadeh, M.; Safarkhani, M.; Ghadiri, A. M.; Kiani, M.; Fatahi, Y.; Taghavimandi, F.; Daneshgar, H.; et al. Bioengineering of CuO Porous (Nano)particles: Role of Surface Amination in Biological, Antibacterial, and Photocatalytic Activity. *Sci. Rep.* **2022**, *12* (1), No. 15351.
(20) Namburi, K. R.; Kora, A. J.; Chetukuri, A.; Kota, V. S. M. K. Biogenic Silver Nanoparticles as an Antibacterial Agent against Bacterial Leaf Blight Causing Rice Phytopathogen *Xanthomonas oryzae* pv. oryzae. *Bioprocess Biosyst. Eng.* **2021**, *44* (9), 1975−1988.
(21) Bankier, C.; Matharu, R. K.; Cheong, Y. K.; Ren, G. G.; Cloutman-Green, E.; Ciric, L. Synergistic Antibacterial Effects of Metallic Nanoparticle Combinations. *Sci. Rep.* **2019**, *9* (1), No. 16074.
(22) Datta Majumdar, T.; Ghosh, C. K.; Mukherjee, A. Dual Role of Copper Nanoparticles in Bacterial Leaf Blight-Infected Rice: A Therapeutic and Metabolic Approach. *ACS Agric. Sci. Technol.* **2021**, *1* (3), 160−172.
(23) Rai, M.; Ingle, A. P.; Pandit, R.; Paralikar, P.; Shende, S.; Gupta, I.; Biswas, J. K.; da Silva, S. S. Copper and Copper Nanoparticles: Role in Management of Insect-Pests and Pathogenic Microbes. *Nanotechnol. Rev.* **2018**, *7* (4), 303−315.
(24) Godymchuk, A.; Frolov, G.; Gusev, A.; Zakharova, O.; Yunda, E.; Kuznetsov, D.; Kolesnikov, E. Antibacterial Properties of Copper Nanoparticle Dispersions: Influence of Synthesis Conditions and Physicochemical Characteristics. *IOP Conf. Ser.: Mater. Sci. Eng.* **2015**, *98* (1), No. 012033.
(25) Ngoc, D. T. B.; Thach, B. D.; Tho, T. P.; Phu, D. V. Effect of Copper Ions Concentration on the Particle Size of Alginate-Stabilized Cu_2O−Cu Nanocolloids and Its Antibacterial Activity against Rice Bacterial Leaf Blight (*Xanthomonas oryzae* pv. oryzae). *Adv. Nat. Sci.: Nanosci. Nanotechnol.* **2021**, *12* (1), No. 013001.
(26) Murthy, H. C. A.; Desalegn, T.; Kassa, M.; Abebe, B.; Assefa, T. Synthesis of Green Copper Nanoparticles Using Medicinal Plant *Hagenia abyssinica* (Brace) J. F. Gmel. Leaf Extract: Antimicrobial Properties. *J. Nanomater.* **2020**, *2020* (1), No. 3924081.
(27) Chaachouay, N.; Azeroual, A.; Benkhnigue, O.; Zidane, L. Alkaloids: A Suitable Precursor for Nanomaterials Synthesis, and Their Various Applications. In *Secondary Metabolites Based Green Synthesis of Nanomaterials and Their Applications*; Springer Nature: Singapore, 2023; pp 23−48.
(28) Ekalu, A.; Habila, J. D. Flavonoids: Isolation, Characterization, and Health Benefits. *Beni-Suef Univ. J. Basic Appl. Sci.* **2020**, *9* (1), No. 45.
(29) Pirsaheb, M.; Gholami, T.; Seifi, H.; Dawi, E. A.; Said, E. A.; Hamoody, A.-H. M.; Altimari, U. S.; Salavati-Niasari, M. Green Synthesis of Nanomaterials by Using Plant Extracts as Reducing and Capping Agents. *Environ. Sci. Pollut. Res.* **2024**, *31* (17), 24768−24787.

(30) Rana, A.; Yadav, K.; Jagadevan, S. A Comprehensive Review on Green Synthesis of Nature-Inspired Metal Nanoparticles: Mechanism, Application and Toxicity. *J. Cleaner Prod.* **2020**, *272*, No. 122880.
(31) Alvarez, A. M.; Toves, P. J.; Vowell, T. S. Bacterial Blight of Anthuriums: Hawaii's Experience with a Global Disease. *APSnet Features* **2006**.
(32) Puławska, J.; Kordyla-Bronka, M.; Jouen, E.; Robène-Soustrade, I.; Gagnevin, L.; Pruvost, O.; Sobiczewski, P.; Orlikowski, L. First Report of Bacterial Blight of Anthurium andreanum in Poland. *Plant Pathol.* **2008**, *57* (4), 775.
(33) Dhanya, M.; Mary, C. Management of Bacterial Blight of Anthurium (Anthurium andreanum Linden.) Using Ecofriendly Materials. *J. Trop. Agric.* **2006**, *44*, 74−75.
(34) Fukui, R.; Fukui, H.; Alvarez, A. Comparisons of Single versus Multiple Bacterial Species on Biological Control of Anthurium Blight. *Phytopathology* **1999**, *89* (5), 366−373.
(35) Norman, D. J.; Ali, G. S. *Anthurium Diseases: Identification and Control in Commercial Greenhouse Operations: PP292/PP292, 3/2012*; EDIS: Gainesville, FL; 2012. https://edis.ifas.ufl.edu/publication/PP292 (accessed Dec 28, 2025).
(36) Committee on Chemical Safety. American Chemical Society. https://www.acs.org/about/governance/committees/chemical-safety.html (accessed Oct 2, 2025).
(37) Powar, N. S.; Patel, V. J.; Pagare, P. K.; Pandav, R. S. Cu Nanoparticle: Synthesis, Characterization and Application. *Chem. Methodol.* **2019**, *3*, 457−480.
(38) Zhang, M.; Chen, Z.; Wang, Y.; Zhang, J.; Zheng, X.; Rao, D.; Han, X.; Zhong, C.; Hu, W.; Deng, Y. Enhanced Light Harvesting and Electron-Hole Separation for Efficient Photocatalytic Hydrogen Evolution over Cu_7S_4-Enwrapped Cu_2O Nanocubes. *Appl. Catal., B* **2019**, *246*, 202−210.
(39) Mardiansyah, D.; Badloe, T.; Triyana, K.; Mehmood, M. Q.; Raeis-Hosseini, N.; Lee, Y.; Sabarman, H.; Kim, K.; Rho, J. Effect of Temperature on the Oxidation of Cu Nanowires and Development of an Easy-to-Produce, Oxidation-Resistant Transparent Conducting Electrode Using a PEDOT:PSS Coating. *Sci. Rep.* **2018**, *8* (1), No. 10639.
(40) Hubbard, C. R.; Snyder, R. L. RIR Measurement and Use in Quantitative XRD. *Powder Diffr.* **1988**, *3* (2), 74−77.
(41) Maduwanthi, R. K.; Munaweera, I.; Perera, W. P. T. D. Nutrient Nanohybrids Based on Sodium Alginate and Carboxymethyl Cellulose Provide Enhanced Slow Release of Magnesium, Zinc and Copper. *Chem. Pap.* **2025**, *79*, 6227.
(42) Jayasinghe, S.; Munaweera, I.; Perera, C.; Siriwardena, D. P.; Kottegoda, N. Low-Carbon-Footprint Plasma-Functionalized Coconut-Coir-Based Porous Carbon as an Efficient and Sustainable Adsorbent. *ChemistrySelect* **2024**, *9* (13), No. e202305164.
(43) Swebocki, T.; Barras, A.; Kocot, A.Minimum Inhibitory Concentration (MIC) and Minimum Bactericidal Concentration (MBC) Assays Using Broth Microdilution Method. 2023 DOI: 10.17504/protocols.io.5qpvo3x6dv4o/v1.
(44) Michelini, L.; Gallina, G.; Capolongo, F.; Ghisi, R. Accumulation and Response of Willow Plants Exposed to Environmentally Relevant Sulfonamide Concentrations. *Int. J. Phytorem.* **2014**, *16* (9), 947−961.
(45) Xu, D.; Pan, H.; Yao, J.; Feng, Y.; Wu, P.; Shao, K. Stress Responses and Biological Residues of Sulfanilamide Antibiotics in *Arabidopsis thaliana*. *Ecotoxicol. Environ. Saf.* **2020**, *199*, No. 110727.
(46) Park, S.; Choi, K. Hazard Assessment of Commonly Used Agricultural Antibiotics on Aquatic Ecosystems. *Ecotoxicology* **2008**, *17* (6), 526−538.
(47) Straub, J. O. Aquatic Environmental Risk Assessment for Human Use of the Old Antibiotic Sulfamethoxazole in Europe. *Environ. Toxicol. Chem.* **2015**, *35* (4), 767−779.
(48) Draviana, H. T.; Fitriannisa, I.; Khafid, M.; Krisnawati, D. I.; Widodo; Lai, C.-H.; Fan, Y.-J.; Kuo, T.-R. Size and Charge Effects of Metal Nanoparticles on Antibacterial Mechanisms. *J. Nanobiotechnol.* **2023**, *21*, 428.
(49) Tiwari, A. K.; Pandey, P. C.; Gupta, M. K.; Narayan, R. J. Nano−Bio Interaction and Antibacterial Mechanism of Engineered Metal Nanoparticles: Fundamentals and Current Understanding. *J. Cluster Sci.* **2025**, *36*, No. 5.
(50) Modi, S. K.; Gaur, S.; Sengupta, M.; Singh, M. S. Mechanistic Insights into Nanoparticle Surface−Bacterial Membrane Interactions in Overcoming Antibiotic Resistance. *Front. Microbiol.* **2023**, *14*, No. 1135579.
(51) Tasnim, N. T.; Ferdous, N.; Rumon, M. M. H.; Shakil, M. S. The Promise of Metal-Doped Iron Oxide Nanoparticles as an Antimicrobial Agent. *ACS Omega* **2024**, *9*, 16−32.
(52) Tavakoli, S.; Kharaziha, M.; Ahmadi, S. Green Synthesis and Morphology-Dependent Antibacterial Activity of Copper Oxide Nanoparticles. *J. Nanostruct.* **2019**, *9* (1), 163−171.
(53) Gudkov, S. V.; Burmistrov, D. E.; Fomina, P. A.; Validov, S. Z.; Kozlov, V. A. Antibacterial Properties of Copper Oxide Nanoparticles. *Int. J. Mol. Sci.* **2024**, *25*, 11563.

https://doi.org/10.1021/acsomega.6c00344
ACS Omega 2026, 11, 25657−25665